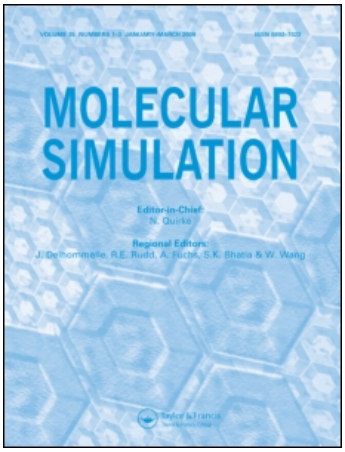

Molecular Simulation
Publication details, including instructions for authors and subscription information:
http://www.informaworld.com/smpp/title~content=t713644482

pH response of conformation of poly(propylene imine) dendrimer in water: a molecular simulation study

Chaofu Wu[a]
[a] Department of Chemistry and Materials Science, Hunan University of Humanities, Science and Technology, Loudi, People's Republic of China

Online publication date: 10 December 2010

To cite this Article Wu, Chaofu(2010) 'pH response of conformation of poly(propylene imine) dendrimer in water: a molecular simulation study', Molecular Simulation, 36: 14, 1164 — 1172
To link to this Article: DOI: 10.1080/08927022.2010.509860
URL: http://dx.doi.org/10.1080/08927022.2010.509860

Molecular Simulation
Vol. 36, No. 14, December 2010, 1164–1172

Taylor & Francis
Taylor & Francis Group

pH response of conformation of poly(propylene imine) dendrimer in water: a molecular simulation study

Chaofu Wu*

Department of Chemistry and Materials Science, Hunan University of Humanities, Science and Technology, Loudi 417000, People's Republic of China

(*Received 11 September 2009; final version received 16 July 2010*)

This work presents the first molecular dynamics simulation of poly(propylene imine) (PPI) dendrimer in explicit water under various pH conditions. The sizes, shapes, surfaces/volumes and density profiles of the PPI dendrimer are analysed. The PPI dendrimer essentially approaches the perfect sphere under all pH conditions, and higher pH leads to more globular structure. The radius of gyration, solvent-accessible surface area (SASA) and solvent-excluded volume (SEV) are all found to increase significantly from high pH to neutral pH and to level thereafter until low pH, which illustrate the dramatic changes in the whole conformation of the dendrimer. These behaviours of the PPI dendrimer quite differ from those of polyamidoamine [Liu, et al. J. Am. Chem. Soc. 2009, 131, 2798–2799], which can be explained by the favourable interactions arising from the additional amide groups. The density profiles have also been calculated to confirm the shifts of density and back-folding of terminals and penetrations of water.

Keywords: pH effects; poly(propylene imine) dendrimer; molecular dynamics simulation

1. Introduction

Dendrimers, as a kind of regular dendritic polymers, exhibit many remarkable properties, such as well-defined structure, monodispersity, polyvalence, low viscosity, which enable the great potentials in DNA delivery, biological reagents, catalysts, nanobiological devices, etc. [1]. Therefore, dendrimers are of great interests both academically and commercially.

Extensive experimental studies have been devoted to elucidating the structure, shape and morphology of dendrimers. However, it has been pointed out that complete experimental characterisation of dendrimers at atomistic level is very difficult, which has lagged the rapid progress in synthesis and design [2]. On the contrary, detailed structural information can be obtained readily from the theoretical and computational techniques, which proved to be the important supplements for the experimental techniques [3]. Among these techniques, molecular simulation methods, in particular molecular dynamics (MD), are very fascinating since they can provide atomistic structure and interactions.

Polyamidoamine (PAMAM) and poly(propylene imine) (PPI) are two of the commercially available dendrimers, which closely resemble each other except the repeating units between the neighbouring branches. The structure of PAMAM dendrimers, either in melts or in solutions, has been extensively studied using the MD simulation method [4–15], where the model systems were refined stepwise to reproduce the experimental observations; surprisingly, only few MD simulations at atomistic level have been carried out on the PPI dendrimer [16–19]. What is more, for these studies, the solvents are in the absence to model the cases of poor solvents. In the practical applications, the dendrimers are generally dissolved into good solvents, i.e. water or methanol. Thus, MD simulations of PPI dendrimers in explicit solvents would be more realistic.

The influence of pH on the size and structure of dendrimers is another important issue, since it is closely related to the utilisation as drug delivery vehicles in physiological environments. A recent study [20] has found that PPI dendrimers are useful in solubility enhancement of amphoteric drugs, and their solubilisation ability can be clearly regulated by pH. The earlier MD simulation study on effects of pH was carried out on the PAMAM dendrimers by Lee and co-workers [4]. This was extended to higher generations in solutions by Maiti [8,10] and Opitz [11] and their co-workers. Inferred from the experiments and confirmed by the recent simulations [14], PAMAM dendrimers undergo pH-responsive conformational changes without swelling. For PPI dendrimers, such MD simulations and experiments have never been carried out previously. However, it has been claimed through the experimental methods that protonation behaviours under various pH are somewhat different for the PPI and PAMAM dendrimers [21–23], which can lead to the different pH response of conformation of PPI dendrimers from the PAMAM dendrimers.

*Corresponding author. Email: xiaowu759@hotmail.com; xiaowu759@qq.com

ISSN 0892-7022 print/ISSN 1029-0435 online

DOI: 10.1080/08927022.2010.509860
http://www.informaworld.com

In a word, the structure of PPI dendrimer in solution has not been completely cleared. As a consequence, this work represents a first report of MD simulation of PPI dendrimer in explicit aqueous solutions. The conformation of the five-generation PPI dendrimer terminated by primary amines (G5-NH_2) is extensively studied. Main focuses are placed on the pH effects on these properties of the dendrimer. These results of PPI dendrimers are compared to those of PAMAM dendrimers reported previously. This work contributes to thoroughly understanding the structure–properties relationship of dendrimers.

2. Computational details

The whole procedure is shown in Figure 1, where the model building and molecular simulations were arranged in two columns. To obtain a reasonable structure, these two kinds of steps were executed alternately. The GROMACS-4.0.5 [24,25] program was employed in parallel for completing most of these calculations except that in the initial stage the commercial Materials Studio-4.0 software (Accelrys Co., San Diego, CA, USA, available at http://accelrys.com/) was used to build a single PPI dendrimer in vacuum.

The model began with building the constituent residues, whose chemical structures are shown in Figure 2, were constructed atom by atom. Such a definition of residues is special, ensuring that the residues had the integral charges 0–2, depending on the protonation state of amine nitrogen atoms. The partial charges were obtained from the COMPASS [26] force field, as tabulated in Tables A1–A3 of Appendix. A single G5-NH_2 PPI dendrimer molecule was built generation by generation based on those residues. After each new generation was built, energy minimisations (EM) were carried out using the steepest descent followed by the conjugate gradient algorithms. The optimised PPI dendrimer molecule was then put into a rhombic dodecahedron box where the periodic boundary conditions and minimum image conventions were imposed. To use the rhombic dodecahedron instead of cubic box is to save volume about 19% [6]. The box whose edges were 1.6 nm (1 nm $= 10^{-9}$ m) away from the solute was big enough to avoid too many interactions from the images. To randomise this bulk system, the quenching and

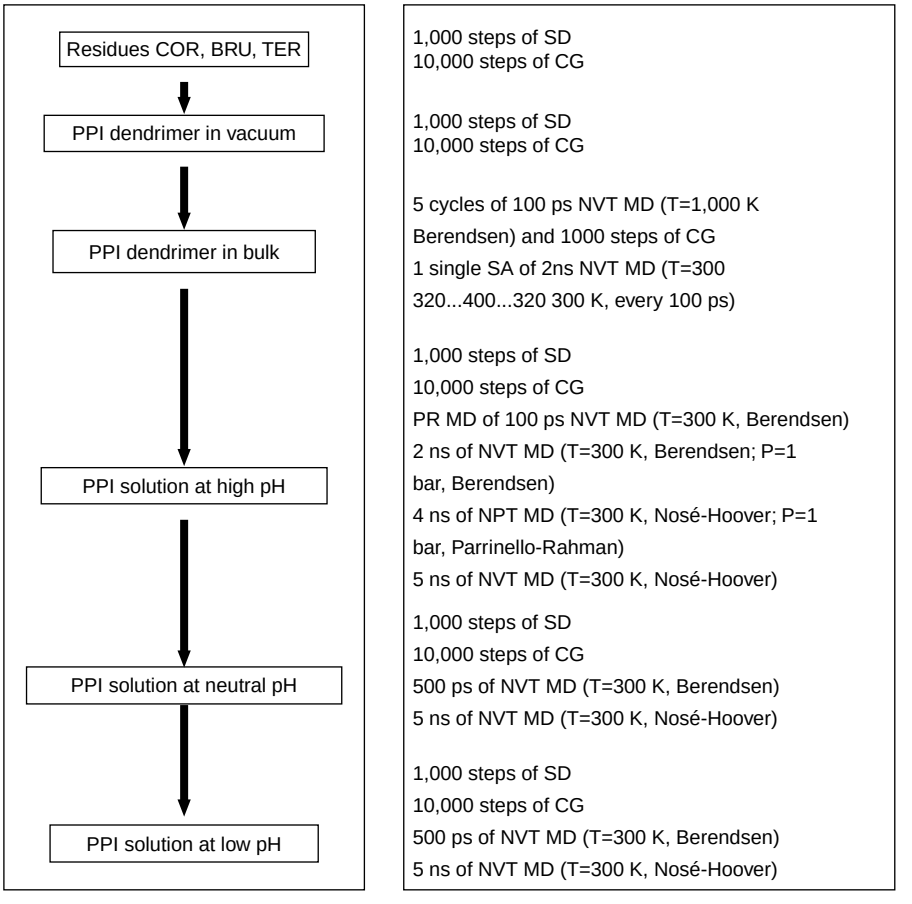

Figure 1. Flow chart of model building (left column) and molecular simulation (right column) in this work.

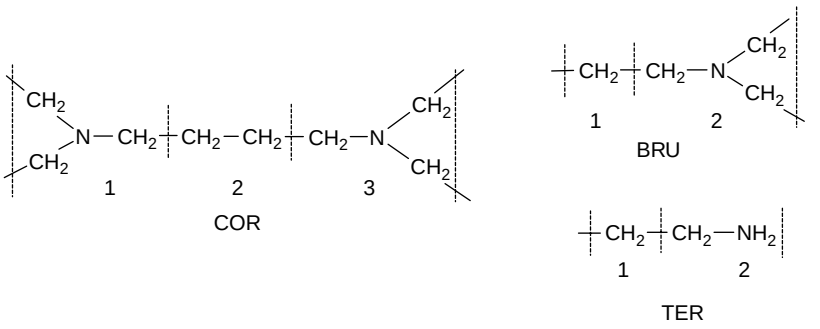

Figure 2. Chemical structure of various residues on G5-NH_2 PPI dendrimer without protonation. For all the residues, the non-hydrogen atoms are named after the element followed by a number, which starts with one and increases from the left to the right or from the top to the bottom. And the hydrogen atoms are named H followed by the number of their bonded non-hydrogen atoms and another number, which differ from each other. The names of all the atoms in the residues are shown in Tables A1–A3 of the Appendix.

annealing procedures were employed using NVT MD and alternatively followed by EM methods. These procedures would ensure to derive an optimised structure for PPI solutions. Another NPT MD simulation was carried out to reach the stable cell volume. One configuration with the cell volume closest to the equilibrium value was chosen for starting all the following simulations.

Essentially, three model systems at three protonation levels were simulated in detail using NVT MD simulation methods. The details of these model systems are shown in Table 1. According to the acid–base titration experiments [21–23], they correspond to three different pH conditions: high pH (>14) with the PPI fully deprotonated (uncharged dendrimer), neutral pH (~10), where all amine groups in odd shells, including the outermost primary amine groups and the odd shells of tertiary amine groups, were protonated, and low pH (~5) with PPI fully protonated. These PPI dendrimers were solvated with the explicit water shell with the thickness 1.5 nm. As for neutral and low pH, the Cl^- counterions with defined number were added to neutralise the negative charges on the dendrimer. These model systems were subjected to a position restrained NVT MD simulation for 100 ps ($1\,ps = 10^{-12}\,s$) so that the solvents and counterions can derive a good disperse around the PPI dendrimers. Subsequently, 5 ns ($1\,ns = 10^{-9}\,s$) of NVT MD simulations without restrains were performed for collecting data, of which the last 2 ns were used to analyse the structure and properties of the model systems.

The original parameters of OPLS-AA [27] force field, except the partial charges, were employed for modelling the interactions in PPI dendrimers. Using the COMPASS charges mixed with the original OPLS-AA parameters was a bit arbitrary. However, the two kinds of charges, except a few terms, were similar in value (Tables A1–A3 of Appendix). Accordingly, TIP4P [28] water was used. To reduce the computational costs, the cut-off and fast particle-mesh Ewald [29] methods were employed for the van der Waals and electrostatics interactions, respectively. In the equilibration phases, the temperature and pressure were controlled by the Berendsen et al. [30] methods. When it came to collecting data, the Nosé–Hoover [31,32] and Parrinello and Rahman [33] methods were employed for coupling the temperature and the pressure, respectively. For all the MD simulations, the leap-frog algorithm was used to update the configuration with the time step of 1 fs ($1\,fs = 10^{-15}\,s$). The last snapshots from the MD simulations were shown in Figure 3 for the three model systems.

3. Results and discussion

By scrutinising the snapshots of trajectories using the VMD-1.8.6 [34] software, some conformation characterisations of PPI dendrimers can be qualitatively learned of, i.e. shape, swelling of size, increase of surface, shifts of density, back-folding of terminals and penetration of water. To quantify these behaviours, some specific properties were computed as follows.

Table 1. Details of model systems for G5-NH_2 PPI solutions under various pH conditions.

pH	No. of PPI atoms	No. of waters	Charge of PPI	No. of Cl^-
High (>14)	1382	3330	0	0
Neutral (~10)	1466	3246	84	84
Low (~5)	1508	3204	126	126

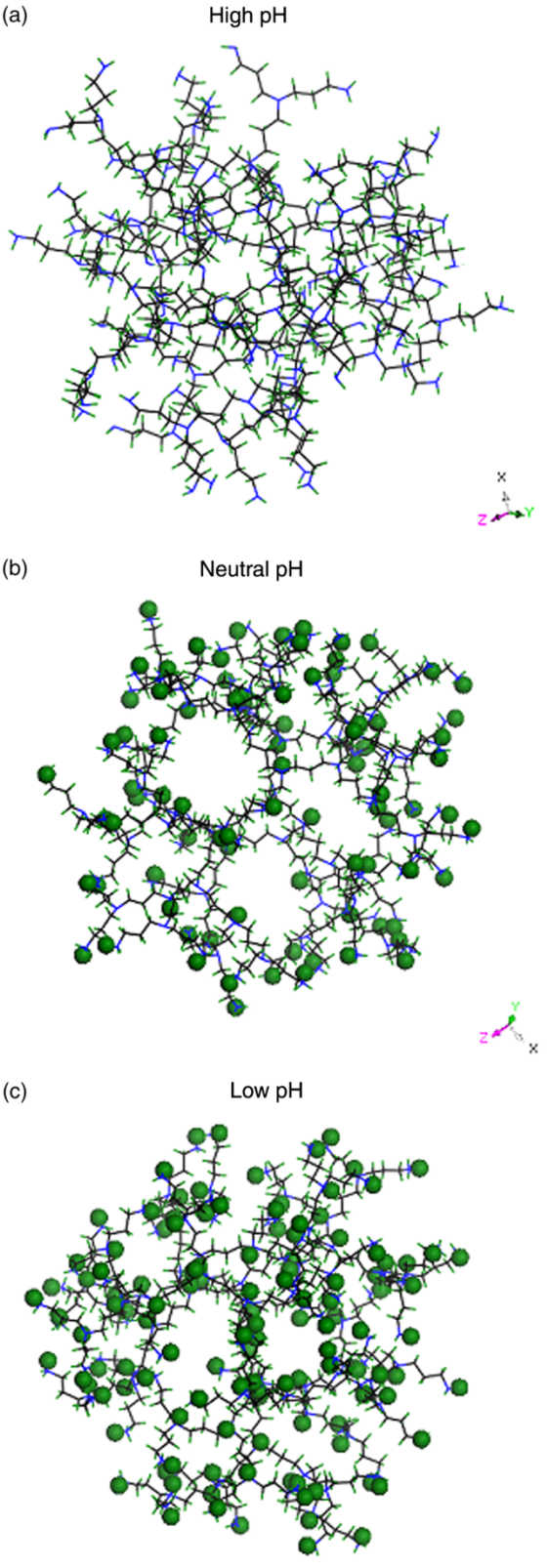

Figure 3. Snapshots of PPI dendrimer at high (a), neutral (b) and low pH (c), the protonated hydrogen atoms are displayed in green CPK ball (colour online).

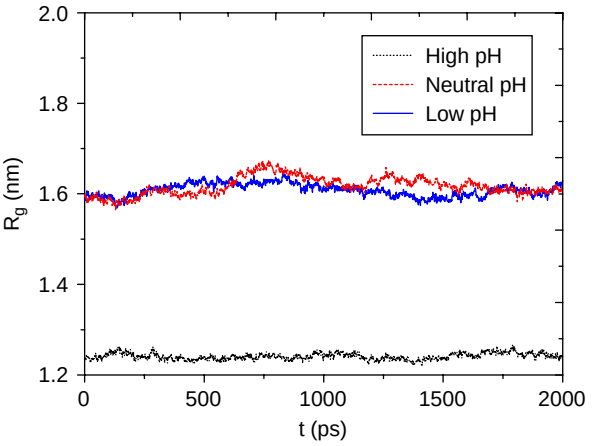

Figure 4. Radii of gyration as function of simulation time for G5-NH_2 PPI dendrimer under various pH conditions.

3.1 *Size of PPI dendrimer*

The size of a dendrimer is an important parameter for almost all its applications. To characterise size of the dendrimer, the radius of gyration R_g is computed according to its definition

$$\langle R_g^2 \rangle = \frac{1}{M} \left\langle \sum_{i=1}^{N} m_i |r_i - R|^2 \right\rangle, \qquad (1)$$

where m_i is the mass of atom i; r_i is the position of atom i; M is the total mass; R is the position of the centre of mass and N is the total number of atoms.

R_g as function of simulation time at the last 2000 ps is presented in Figure 4 for the three pH conditions. It can be obviously seen that the simulation time is long enough to attain the equilibrium values. The results as obtained by averaging over the last 2000 ps are represented in Table 2. For the high pH condition, the computed R_g is 1.234 ± 0.007 nm, which compares well with other simulated value 1.25 nm using the original CVFF force field [16]. However, the different simulation conditions, i.e. with explicit water in this work and without any water in their work, make this comparison hard. In practice, the experimental value as obtained by SANS is reported as 1.39 nm [16]. Note also that the SANS was performed on 1% aqueous solutions whereas this simulation was carried out on about 10% aqueous solution. Less good solvent (i.e.

Table 2. Specific properties of the G5-NH_2 PPI dendrimer in water under various pH conditions.

pH	R_g (nm)	δ	SASA (nm^2)	SEV (nm^3)
High (>14)	1.234 ± 0.007	0.0027	75.53	15.4
Neutral (~10)	1.599 ± 0.014	0.0059	127.41	18.2
Low (~5)	1.583 ± 0.018	0.0091	125.19	18.2

water) can swell the dendrimer less, leading to the lower R_g. Therefore, the employed model and algorithm can be considered acceptable.

For the neutral and low pH conditions, no corresponding experimental or simulation data are available for direct comparisons. However, only the R_g values at these two pH conditions are independent of pH, which show a significant increase (~30%) from the high pH. Such a trend of PPI dendrimer is quite different from that of PAMAM dendrimer [14]. It can be explained that it is the additional amide groups that cause the difference. Namely, such amide groups on the PAMAM dendrimer tend to form adequate hydrogen bonds (HB), which can cancel the partial influence of additional repulsion interactions arising from the protonation of amine groups. Brocorens and co-workers [19] found amide-terminated PPI dendrimers adopt morphologies with the higher number of HBs possible than amine-terminated PPI dendrimers, which seems to support this assumption. Nevertheless, this issue deserves a further direct investigation. It should also be noted that a further titration (i.e. at pH = 5) would not change the size of the dendrimer significantly since at pH = 10, the PPI dendrimer has approached the extended limit.

3.2 Shape of PPI dendrimer

In general, high generation dendrimers approach spherical shape. Therefore, asphericity or relative shape anisotropy is frequently used to quantify the shape of a dendrimer, which is estimated as

$$\delta = 1 - 3\frac{\left\langle \sum_{i\neq j} I_i I_j \right\rangle}{\left\langle \sum_i I_i^2 \right\rangle}, \qquad (i,j = x,y,z), \qquad (2)$$

where I_x, I_y and I_z are the principal moments of the equivalent ellipsoid. When the shape of a dendrimer is perfectly spherical, this quantity assumes the value of 0.

The asphericity of PPI dendrimers in aqueous solutions is also shown in Table 2 for various pH conditions. It can be seen that under all pH conditions, the PPI dendrimer is close to the perfect spherical ones, indicating the high flexibility of chains. Moreover, a higher pH leads to a more globular structure. This can be considered as a consequence of additional electrostatic repulsion between protonated primary and tertiary amines. Zacharopoulos and Economou [18] has ever reported a value about 0.10 for the G5 PPI dendrimer in the melt, which shows less spherical shape than the same dendrimer in the solution. This confirms Maiti's opinions that the favourable interactions with the solvent make the shape of the dendrimer more spherical compared to the case with no solvent [8].

3.3 SASA/SEV of PPI dendrimer

For applications of dendrimers, surface area and internal volume are two more important properties than size and shape, which can be defined by the solvent-accessible surface area (SASA) and solvent-excluded volume (SEV), respectively. The double cubic lattice method (DCLM) [35] was employed for these calculations, where the radius 0.14 nm of probe (H_2O) and 24 dots per sphere were adopted.

The calculated results of SASA and SEV at various pH conditions are also tabulated in Table 2. It can be seen that the SASA increases by 68.6% from high to neutral pH and levels from neutral pH to low pH, while the SEV increases by 18.2% and levels between the two sections, respectively. Bigger SASA at both neutral and low pH indicates the great potentials of PPI dendrimer utilised as catalysis. The significant increase in SASA and SEV implies more interactions to occur between the PPI dendrimer and water, which are in good agreement with the variations of R_g. This behaviour illustrates the dramatic change in the entire conformation, i.e. from tension to looseness. Note that this vision of the PPI dendrimer quite differs from that of PAMAM dendrimer in that the latter indicates a moderate decrease in SASA and SEV [14]. Once again, this difference can be related to the amide groups between the neighbour branches on the PAMAM dendrimers.

3.4 Density profiles of PPI dendrimer

The average radial density $\rho(r)$ provides a more detailed descriptor for the conformation of dendrimer, which is defined as the number of atoms divided by the volume $r^2\,dr$ within the spherical shell of radius r and thickness dr. Thus, the integration over r from 0 to R would yield the total number of atoms $N(R)$ at distance R from the centre of mass of dendrimer

$$N(R) = 4\pi\int_0^R \rho(r) r^2\,dr. \qquad (3)$$

It can be inferred that smaller thickness of concentric shells would be too noisy [6]. Therefore, 0.1 nm is employed in the calculations. Moreover, the first three shells (up to ~0.3 nm) have been omitted because they only contain a few atoms in the too small volume of shells which can lead to highly inaccuracy [16].

Figure 5(a) represents the radial density distributions of PPI dendrimers for the three pH. Some common features can be found for all: (1) total density shows two maxima and a minimum between them, just like a spike; (2) the first maximum is at around 0.3 nm away from the core, meaning a 'dense-core' structure; (3) the minimum is located at 0.6 nm away from the core and (4) the second maximum

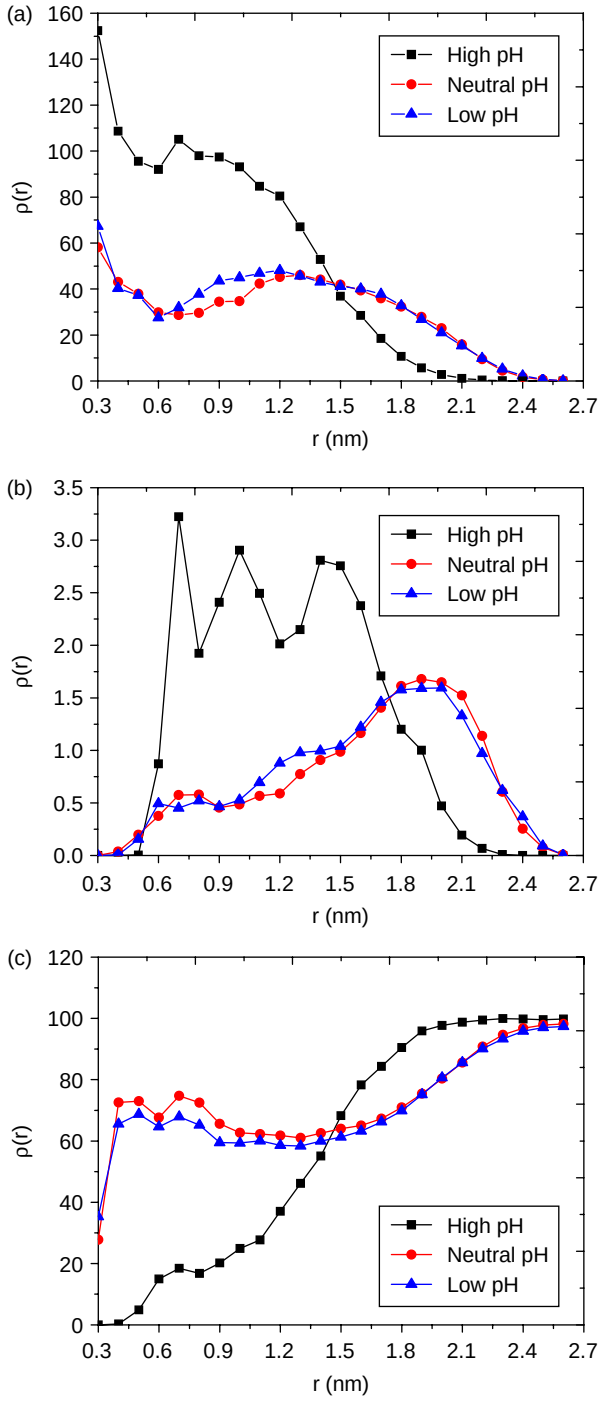

Figure 5. Radial density profiles of all atoms (a) and primary amine nitrogen atoms (b) on the G5-NH_2 PPI dendrimer, and all atoms on water (c).

is followed by a monotone decay to 0. The shapes of these density profiles support the assumption that many cavities are located in the dendrimer, as shown in Figure 3, which are the basis of many desirable applications. Note also the second maximum density of the PPI dendrimer shifts from 0.7 nm at high pH to 1.2–1.3 nm at neutral or low pH. In the pH-responsive behaviour, PPI dendrimer closely resembles PAMAM dendrimer [14], which suggests that the conformation changes from a 'dense core' (high pH) to a 'dense shell' (low pH). This seems reasonable that pH can be used as a trigger for hosting or releasing small molecules such as drugs in the drug delivery.

Figure 5(b) shows the density profiles of terminal nitrogen atoms on PPI dendrimer under the three pH conditions. These distribution functions nicely illustrate that the amine end groups are distributed throughout the dendrimer molecule. Specially, at high pH, the density profile of PPI dendrimer exhibits a plateau region covering three peaks, followed by a monotonic decrease in the density towards the exterior of the molecule, which is closely similar to that of PAMAM dendrimer [8]. The highest peak at distance about 0.7 nm from the core indicates that there is significant back-folding of the outer subgeneration throughout the interior of the molecules. However, when pH is either neutral or low, the density profile behaves just like climbing a ladder with three pedals corresponding to the three broad peaks, which implies that terminal amine groups prefer to be located at the periphery of the molecules. This picture is in accord with the swelling of the PPI dendrimer as suggested by the radius of gyration.

Figure 5(c) plots the density profiles of water molecules around the centre of mass of PPI dendrimer for various pH. It can be obviously observed that many water molecules have penetrated throughout the interior of the dendrimer (Figure 5(a)). For all the three conditions, it can be found that before reaching the bulk density of water an abrupt increase in density takes place at the distance equal to the corresponding radius of gyration. The density profiles of both neutral and low pH are essentially similar to each other, except that the former is a slight higher than the latter. However, at the same distance up to 1.4 nm, the densities of both neutral and low pH are much higher than that of the high pH, indicating that more water molecules have been encapsulated into the interior of dendrimer.

4. Conclusions

MD simulations at atomistic level have been carried out on aqueous solutions of PPI G5-NH_2 dendrimer under a wide pH ranging from 14 to 5. The energies, densities and in particular radii of gyration suggest that all the model systems have been brought into equilibrium, which indicate the superiority of the adopted stepwise strategy, i.e. quenching and annealing. Generally, the calculated properties compared well with the limited experimental and simulation data, which validate the OPLS-AA and TIP4P force fields as well as the partial charges. For all pH conditions, the PPI dendrimer in essence approaches the perfect sphere, and higher pH leads to more globular structure. With the variation of pH from high to neutral

or low, the radius of gyration, SASA and SEV exhibit significant increase, which illustrate the dramatic change in the whole conformation of PPI dendrimer, i.e. from tension to looseness. These behaviours of the PPI dendrimers are quite different from those of PAMAM dendrimers in that the latter undergo conformation change without swelling. These differences can be traced to the additional interactions arising from the amide groups between the neighbour branches on the PAMAM dendrimers. This issue deserves a further investigation in the future. The density profiles of all atoms and terminal nitrogen atoms on PPI dendrimers and all atoms of water molecules confirm the shifts of density and back-folding of terminals and penetrations of water, as found for many other dendrimers. These characterisations seem to indicate the great potentials of PPI dendrimers employed in drug convey and catalysis. More simulations or experiments combined with theories are required to realise these applications since this is the first MD simulations of PPI dendrimers in explicit water solutions under various pH conditions.

Acknowledgements

The author is indebted to the Molecular Simulation Centre of Hunan Province (at Hunan University) and Henan University of Urban Construction, which provided the commercial software (Materials Studio-4.0) and hardware for completing this work. The author also wishes to acknowledge his wife, Mrs Wanhua Yang, for the sustained encouragement and support, and their daughter Jing Wu for bringing many joys to the family and motivating some good ideas in his mind.

References

[1] F. Vogtle, G. Richardt, and N. Werner, *Dendrimer Chemistry*, Wiley-VCH Verlag, Weinheim, 2009.

[2] C. Jana, G. Jayamurugan, R. Ganapathy, P.K. Maiti, N. Jayaraman, and A.K. Sood, *Structure of poly(propyl ether imine) dendrimer from fully atomistic molecular dynamics simulation and by small angle X-ray scattering*, J. Chem. Phys. 124 (2006), 204719–204728.

[3] M. Ballauff and C.N. Likos, *Dendrimers in solution: Insight from theory and simulation*, Angew. Chem., Int. Ed. 43 (2004), pp. 2998–3020.

[4] I. Lee, B.D. Athey, A.W. Wetzel, W. Meixner, and J.R. Baker, Jr, *Structural molecular dynamics studies on polyamidoamine dendrimers for a therapeutic application: Effects of pH and generation*, Macromolecules 35 (2002), pp. 4510–4520.

[5] P.K. Maiti, T. Cagin, G. Wang, and W.A. Goddard, III, *Structure of PAMAM dendrimers: Generations 1 through 11*, Macromolecules 37 (2004), pp. 6236–6254.

[6] M. Han, P. Chen, and X. Yang, *Molecular dynamics simulation of PAMAM dendrimer in aqueous solution*, Polymer 46 (2005), pp. 3481–3488.

[7] S.-T. Lin, P.K. Maiti, and W.A. Goddard, III, *Dynamics and thermodynamics of water in PAMAM dendrimers at subnanosecond time scales*, J. Phys. Chem. B 109 (2005), pp. 8663–8672.

[8] P.K. Maiti, T. Cagin, S.-T. Lin, and W.A. Goddard, III, *Effect of solvent and pH on the structure of PAMAM dendrimers*, Macromolecules 38 (2005), pp. 979–991.

[9] Y. Peng and G.A. Kaminski, *Accurate determination of pyridine-poly(amidoamine) dendrimer absolute binding constants with the OPLS-AA force field and direct integration of radial distribution functions*, J. Phys. Chem. B 109 (2005), pp. 15145–15149.

[10] P.K. Maiti, and W.A. Goddard, III, *Solvent quality changes the structure of G8 PAMAM dendrimer, a disagreement with some experimental interpretations*, J. Phys. Chem. B 110 (2006), pp. 25628–25632.

[11] A.W. Opitz and N.J. Wagner, *Structural investigations of poly(amido amine) dendrimers in methanol using molecular dynamics*, J. Polym. Sci. Part B 44 (2006), pp. 3062–3077.

[12] P.M.R. Paulo, J.N.C. Lopes, and S.M.B. Costa, *Molecular dynamics simulations of charged dendrimers: Low-to-intermediate half-generation PAMAMs*, J. Phys. Chem. B 111 (2007), pp. 10651–10664.

[13] P. Carbone and F. Muller-Plathe, *Molecular dynamics simulations of polyaminoamide (PAMAM) dendrimer aggregates: Molecular shape, hydrogen bonds and local dynamics*, Soft Matter 5 (2009), pp. 2638–2647.

[14] Y. Liu, V.S. Bryantsev, M.S. Diallo, and W.A. Goddard, III, *PAMAM dendrimers undergo pH responsive conformational changes without swelling*, J. Am. Chem. Soc. 131 (2009), pp. 2798–2799.

[15] I. Tanis and K. Karatasos, *Association of a weakly acidic anti-inflammatory drug (Ibuprofen) with a poly(amidoamine) dendrimer as studied by molecular dynamics simulations*, J. Phys. Chem. B 113 (2009), pp. 10984–10993.

[16] R. Scherrenberg, B. Coussens, P.v. Vliet, G. Edouard, J. Brackman, E.d. Brabander, and K. Mortensen, *The molecular characteristics of poly(propyleneimine) dendrimers as studied with small-angle neutron scattering, viscosimetry, and molecular dynamics*, Macromolecules 31 (1998), pp. 456–461.

[17] E. Blasizza, M. Fermeglia, and S. Pricl, *Dendrimers as functional materials. A molecular simulation study of poly(propylene) imine starburst molecules*, Mol. Simul. 24 (2000), pp. 167–189.

[18] N. Zacharopoulos and I.G. Economou, *Morphology and organization of poly(propylene imine) dendrimers in the melt from molecular dynamics simulation*, Macromolecules 35 (2002), pp. 1814–1821.

[19] P. Brocorens, R. Lazzaroni, and J.-L. Brédas, *The conformation of amine- and amide-terminated poly(propylene imine) dendrimers as investigated by molecular simulation methods*, J. Phys. Chem. B 109 (2005), pp. 19897–19907.

[20] U. Gupta, H.B. Agashe, and N.K. Jain, *Polypropylene imine. Dendrimer mediated solubility enhancement: Effect of pH and functional groups of hydrophobes*, J. Pharm. Pharm. Sci. 10 (2007), pp. 358–367.

[21] G.J.M. Koper, M.H.P.v. Genderen, C. Elissen-Roman, M.W.P.L. Baars, E.W. Meijer, and M. Borkovec, *Protonation mechanism of poly(propylene imine) dendrimers and some associated oligo amines*, J. Am. Chem. Soc. 119 (1997), pp. 6512–6521.

[22] R.C.V. Duijvenbode, M. Borkovec, and G.J.M. Koper, *Acid-base properties of poly(propylene imine) dendrimers*, Polymer 39 (1998), pp. 2657–2664.

[23] D. Cakara, J. Kleimann, and M. Borkovec, *Microscopic protonation equilibria of poly(amidoamine) dendrimers from macroscopic titrations*, Macromolecules 36 (2003), pp. 4201–4207.

[24] D.v.d. Spoel, E. Lindahl, B. Hess, G. Groenhof, A.E. Mark, and H.J.C. Berendsen, *Gromacs: Fast, flexible, and free*, J. Comput. Chem. 26 (2005), pp. 1701–1718.

[25] B. Hess, C. Kutzner, D.v.d. Spoel, and E. Lindahl, *Gromacs 4: Algorithms for highly efficient, load-balanced, and scalable molecular simulation*, J. Chem. Theory Comput. 4 (2008), pp. 435–447.

[26] H. Sun, *Compass: An* ab initio *force-field optimized for condensed-phase applications overview with details on alkane and benzene compounds*, J. Phys. Chem. B 102 (1998), pp. 7338–7364.

[27] W.L. Jorgensen, D.S. Maxwell, and J. Tirado-Rives, *Development and testing of the Opls all-atom force field on conformational energetics and properties of organic liquids*, J. Am. Chem. Soc. 118 (1996), pp. 11225–11236.

[28] W.L. Jorgensen, J. Chandrasekhar, J.D. Madura, R.W. Impey, and M.L. Klein, *Comparison of simple potential functions for simulating liquid water*, J. Chem. Phys. 79 (1983), pp. 926–935.

[29] T. Darden, D. York, and L. Pedersen, *Particle mesh Ewald: An* N*Log*(N*) method for Ewald sums in large systems*, J. Chem. Phys. 98 (1993), pp. 10089–10092.
[30] H.J.C. Berendsen, J.P.M. Postma, W.F. van Gunsteren, A. DiNola, and J.R. Haak, *Molecular dynamics with coupling to an external bath*, J. Chem. Phys. 81 (1984), pp. 3684–3690.
[31] S. Nosé, *A unified formulation of the constant temperature molecular dynamics methods*, J. Chem. Phys. 81 (1984), pp. 511–519.
[32] W.G. Hoover, *Canonical dynamics: Equilibrium phase-space distributions*, Phys. Rev. A. 31 (1985), pp. 1695–1697.
[33] M. Parrinello and A. Rahman, *Polymorphic transitions in single crystals: A new molecular dynamics method*, J. Appl. Phys. 52 (1981), pp. 7182–7190.
[34] W. Humphrey, A. Dalke, and K. Schulten, *VMD-visual molecular dynamics*, J. Mol. Graph. 14 (1996), pp. 33–38.
[35] F. Eisenhaber, P. Lijnzaad, P. Argos, C. Sander, and M. Scharf, *The double cubic lattice method: Efficient approaches to numerical integration of surface area and volume and to dot surface contouring of molecular assemblies*, J. Comput. Chem. 16 (1995), pp. 273–284.

Appendix

Table A1. Atom types and partial atom charges of protonated and deprotonated COR residues.

Deprotonated				Protonated			
Atom	Atom type OPLS-AA	Partial charge COMPASS	Partial charge OPLS-AA	Atom	Atom type OPLS-AA	Partial charge COMPASS	Partial charge OPLS-AA
C1	Opls_908	0.081	0.09	C1	opls_943	0.301	0.15
H11	Opls_911	0.053	0.06	H11	opls_911	0.053	0.06
H12	Opls_911	0.053	0.06	H12	opls_911	0.053	0.06
C2	Opls_908	0.081	0.09	C2	opls_943	0.301	0.15
H21	Opls_911	0.053	0.06	H21	opls_911	0.053	0.06
H22	Opls_911	0.053	0.06	H22	opls_911	0.053	0.06
N3	Opls_902	−0.561	−0.63	N3	opls_940	−0.501	−0.1
–	–	–	–	H31	opls_941	0.280	0.29
C4	Opls_908	0.081	0.09	C4	opls_943	0.301	0.15
H41	Opls_911	0.053	0.06	H41	opls_911	0.053	0.06
H42	Opls_911	0.053	0.06	H42	opls_911	0.053	0.06
C5	Opls_136	−0.106	−0.12	C5	opls_136	−0.106	−0.12
H51	Opls_140	0.053	0.06	H51	opls_140	0.053	0.06
H52	Opls_140	0.053	0.06	H52	opls_140	0.053	0.06
C6	Opls_136	−0.106	−0.12	C6	opls_136	−0.106	−0.12
H61	Opls_140	0.053	0.06	H61	opls_140	0.053	0.06
H62	Opls_140	0.053	0.06	H62	opls_140	0.053	0.06
C7	Opls_908	0.081	0.09	C7	opls_943	0.301	0.15
H71	Opls_911	0.053	0.06	H71	opls_911	0.053	0.06
H72	Opls_911	0.053	0.06	H72	opls_911	0.053	0.06
N8	Opls_902	−0.561	−0.63	N8	opls_940	−0.501	−0.1
–	–	–	–	H81	opls_941	0.280	0.29
C9	Opls_908	0.081	0.09	C9	opls_943	0.301	0.15
H91	Opls_911	0.053	0.06	H91	opls_911	0.053	0.06
H92	Opls_911	0.053	0.06	H92	opls_911	0.053	0.06
CA	Opls_908	0.081	0.09	CA	opls_943	0.301	0.15
HA1	Opls_911	0.053	0.06	HA1	opls_911	0.053	0.06
HA2	Opls_911	0.053	0.06	HA2	opls_911	0.053	0.06
Σ	–	0	0	Σ	–	2	2

Table A2. Atom types and partial atom charges of protonated and deprotonated BRU residues.

Deprotonated				Protonated			
Atom	Atom type OPLS-AA	Partial charge COMPASS	Partial charge OPLS-AA	Atom	Atom type OPLS-AA	Partial charge COMPASS	Partial charge OPLS-AA
C1	Opls_136	−0.106	−0.12	C1	opls_136	−0.106	−0.12
H11	Opls_140	0.053	0.06	H11	opls_140	0.053	0.06
H12	Opls_140	0.053	0.06	H12	opls_140	0.053	0.06
C2	Opls_908	0.081	0.09	C2	opls_943	0.301	0.15
H21	Opls_911	0.053	0.06	H21	opls_911	0.053	0.06
H22	Opls_911	0.053	0.06	H22	opls_911	0.053	0.06
N3	Opls_902	−0.561	−0.63	N3	opls_940	−0.501	−0.10
–	–	–	–	H31	opls_941	0.280	0.29
C4	Opls_908	0.081	0.09	C4	opls_943	0.301	0.15
H41	Opls_911	0.053	0.06	H41	opls_911	0.053	0.06
H42	Opls_911	0.053	0.06	H42	opls_911	0.053	0.06
C5	Opls_908	0.081	0.09	C5	opls_943	0.301	0.15
H51	Opls_911	0.053	0.06	H51	opls_911	0.053	0.06
H52	Opls_911	0.053	0.06	H52	opls_911	0.053	0.06
Σ	–	0	0	Σ	–	1	1

Table A3. Atom types and partial atom charges of protonated and deprotonated TER residues.

Deprotonated				Protonated			
Atom	Atom type OPLS-AA	Partial charge COMPASS	Partial charge OPLS-AA	Atom	Atom type OPLS-AA	Partial charge COMPASS	Partial charge OPLS-AA
C1	Opls_136	−0.106	−0.12	C1	opls_136	−0.106	−0.12
H11	Opls_140	0.053	0.06	H11	opls_140	0.053	0.06
H12	Opls_140	0.053	0.06	H12	opls_140	0.053	0.06
C2	Opls_906	0.081	0.06	C2	opls_292	0.301	0.19
H21	Opls_911	0.053	0.06	H21	opls_911	0.053	0.06
H22	Opls_911	0.053	0.06	H22	opls_911	0.053	0.06
N3	Opls_900	−0.893	−0.9	N3	opls_287	−0.247	−0.3
H31	Opls_909	0.353	0.36	H31	opls_290	0.280	0.33
H32	Opls_909	0.353	0.36	H32	opls_290	0.280	0.33
–	–	–	–	H33	opls_290	0.280	0.33
Σ	–	0	0	Σ	–	1	1